

Molecular functionalization of NiO nanocatalyst for enhanced water oxidation by electronic structure engineering

Lizhou Fan,¹ Dr. Biaobiao Zhang,¹ Dr. Zhen Qiu,² Dr. N. V. R. Aditya Dharanipragada³, Dr. Brian J.J. Timmer,¹ Dr. Fuguo Zhang,¹ Dr. Xia Sheng,¹ Tianqi Liu,¹ Qijun Meng,¹ Dr. A. Ken Inge³, Prof. Tomas Edvinsson,² Prof. Licheng Sun^{1,4,5*}

¹ *Department of Chemistry, KTH Royal Institute of Technology, 10044 Stockholm, Sweden*

² *Department of Engineering Sciences, Solid State Physics, Uppsala University, Box 534, 75121 Uppsala, Sweden*

³ *Department of Materials and Environmental Chemistry, Stockholm University, 10691 Stockholm, Sweden*

⁴ *State Key Laboratory of Fine Chemicals, Institute of Artificial Photosynthesis, DUT-KTH Joint Education and Research Center on Molecular Devices, Dalian University of Technology (DUT), 116024 Dalian, China*

⁵ *Center of Artificial Photosynthesis for Solar Fuels, School of Science, Westlake University, 310024 Hangzhou, China*

**Corresponding author Email: lichengs@kth.se*

Abstract:

Tuning the local environment of nanomaterial-based catalysts has emerged as an effective approach to optimize their oxygen evolution reaction (OER) performance, yet the controlled electronic modulation around surface active sites remains a grand challenge. Herein, we achieve directed electronic modulation of NiO nanoparticles by simple surface molecular modification with small organic molecules. By adjusting the electronic properties of modifying molecules, the local electronic structure is rationally tailored and a close electronic structure-activity relationship is discovered: the increasing electron-withdrawing modification readily decreases the electron density around surface Ni sites, accelerating the reaction kinetics and improving OER activity, and vice versa. Detailed investigation by *operando* Raman spectroelectrochemistry revealed that the electron-withdrawing modification facilitates the charge transfer kinetics, stimulates the catalyst reconstruction, and promotes abundant high-valent γ -NiOOH reactive species generation. The NiO-C₆F₅ catalyst, with the optimized electronic environment, exhibits superior performance towards water oxidation. This work provides a well-designed and effective approach for heterogeneous catalyst fabrication under the molecular level.

Keywords: Water oxidation, electrocatalysis, molecular modification, nanomaterials, catalyst self-reconstruction

Introduction

The oxygen evolution reaction (OER) plays a pivotal role as the “anodic half-reaction” in sustainable energy conversion strategies, such as electrochemical water splitting, CO₂ reduction, and nitrogen reduction.^[1] Limited by the multi-proton coupled electron transfer process, the OER suffers from sluggish kinetics and is the bottleneck for most renewable energy systems. To lower the OER overpotential, first-row transition-metal oxides have been investigated as cost-effective heterogeneous catalysts over the past years. Plenty of studies suggested that the local structure around surface active sites is essential to heterogeneous catalysis.^[1a, 2] Adjustment of the local environment is thus considered an effective approach to improve the OER activity.

To date, two approaches have been developed for local electronic modulation on OER catalysts, including heteroatom doping and defect engineering. Several efficient OER catalysts have been fabricated by these methods, such as NiFe, CoFe, NiFeCr, NiV catalysts.^[3] However, since these methodologies are mainly based on bulk materials modification, it remains challenging to rationally tailor the local electronic structure at catalyst surface, which can directly impact the OER catalysis at the electrocatalyst/electrolyte interface. Moreover, the structural complexity of multi-metal OER catalysts renders it difficult to gain deeper mechanistic understanding, e.g., the identification of the real active center, the investigation of electronic structure-activity relationships.^[4] In addition, recent reports revealed that a self-reconstruction of catalyst commonly occurs at catalyst surfaces during the OER process, deriving the oxy(hydroxide) layer as the true OER active phase.^[5] It is thus highly favorable to rationally adjust the surface electronic structure of the catalyst, and thereby directly influence the catalyst reconstruction, tuning the OER activity. Hence, exploration of simple and effective strategies for directed electronic modulation at catalyst surface are greatly desired.

In this work, we turn to molecular functionalization approach to rationally modulate the surface electronic structure of NiO nanocatalyst, and thereby directly tailor the catalyst self-reconstruction process, improving the OER activity. Through the covalent grafting reaction between organic diazonium salts and metal oxides, ultrasmall (1~3 nm) NiO nanoparticles are functionalized with a series of aryl groups bearing different substituents (Fig. 1). By adjusting the electronic properties of

the substituents, the electronic structure around surface Ni sites has been explicitly modulated and the OER activity has been systematically regulated, *i.e.*, the introduction of electron-withdrawing groups decreases the electron density around Ni and improves the OER activity, and vice versa. Detailed investigations indicated that the strong electron-withdrawing molecular modification affects the charge transfer kinetics and facilitates the catalyst surface reconstruction, generating abundant γ -NiOOH active phase. The NiO-C₆F₅ catalyst, possessing the strongest electron-withdrawing functionalization, exhibits superior performance towards OER.

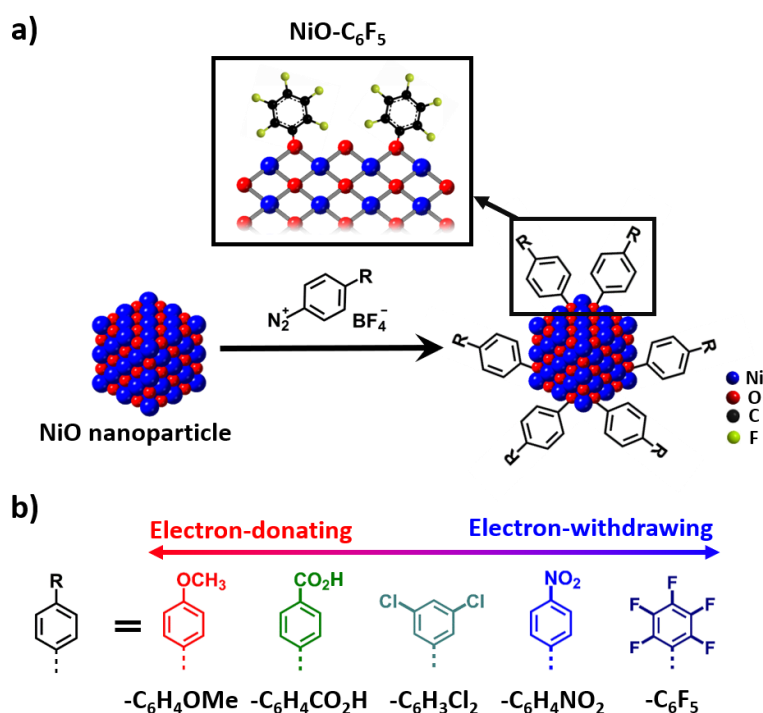


Figure 1 a) Schematic presentation of the molecular modification process on NiO nanoparticles, inset: the local surface structure of NiO-C₆F₅. b) Schematic presentation of the aryl groups with different electronic properties used as molecular modification.

Results and Discussion

Ultrasmall NiO nanoparticles were synthesized as a model heterogeneous OER catalyst, as the small particle size is expected to enlarge the catalyst surface area, promote coordinatively unsaturated site exposure, and facilitate the surface molecular modification via covalent bonds.^[6] The HRTEM image

of the obtained NiO sample shows non-aggregated ultrasmall nanoparticles with particle size of 1-3 nm (Fig. 2a and S3), and the XRD pattern presents typical nickel oxide diffraction peaks at 37.2°, 43.2°, 62.8° (Fig. S1). Based on the XRD peak width, the averaged particle size was calculated to be 2.4 nm, illustrating the formation of ultrasmall NiO nanocrystals.^[7]

A series of aryl-groups with different substitution were introduced to the NiO nanoparticle surface through the grafting reaction between diazonium salts and nickel oxide (Fig. 1a).^[8] The substitution groups were adjusted to be 4-MeO-, 4-CO₂H-, 3,5-Cl₂-, 4-NO₂- and 2,3,4,5,6-F₅-groups, giving molecularly modified samples of NiO-C₆H₄OMe, NiO-C₆H₄CO₂H, NiO-C₆H₃Cl₂, NiO-C₆H₄NO₂ and NiO-C₆F₅ (Fig. 1b). Dictated by the varied Hammett parameters of substitutions, the electronic property of modifying aryl-groups can be systematically regulated: the highest Hammett parameter (0.98) of 2,3,4,5,6-F₅ demonstrates the strongest electron-withdrawing ability of -C₆F₅ group in this series, while the lowest Hammett parameter (-0.27) of 4-MeO- expresses the highest electron-donating property of the -C₆H₄OMe group (Fig. S5).^[9] The different electronic features of the molecular modification is expected to distinctively influence the local electronic environment at NiO nanoparticles surface.

XRD, TEM, and HRTEM were firstly performed to characterize the crystalline structure of modified NiO samples. The XRD pattern of all modified NiO samples show typical NiO diffraction patterns, without apparent peak change compared with the parent NiO nanoparticles (Fig. S6). The TEM images display ultrasmall nanoparticles with particle sizes of 1~4 nm, and the HRTEM images show distinct lattice fringes with an interplanar spacing of 0.21 nm (Fig. S7, S8, S9, S10 and S11). No obvious particle aggregation or surface amorphicity was observed after molecular modification. The TEM-EDS spectra of NiO-C₆F₅ and NiO-C₆H₃Cl₂ samples exhibit distinct F and Cl fluorescence signals, illustrating the successful molecular modification.

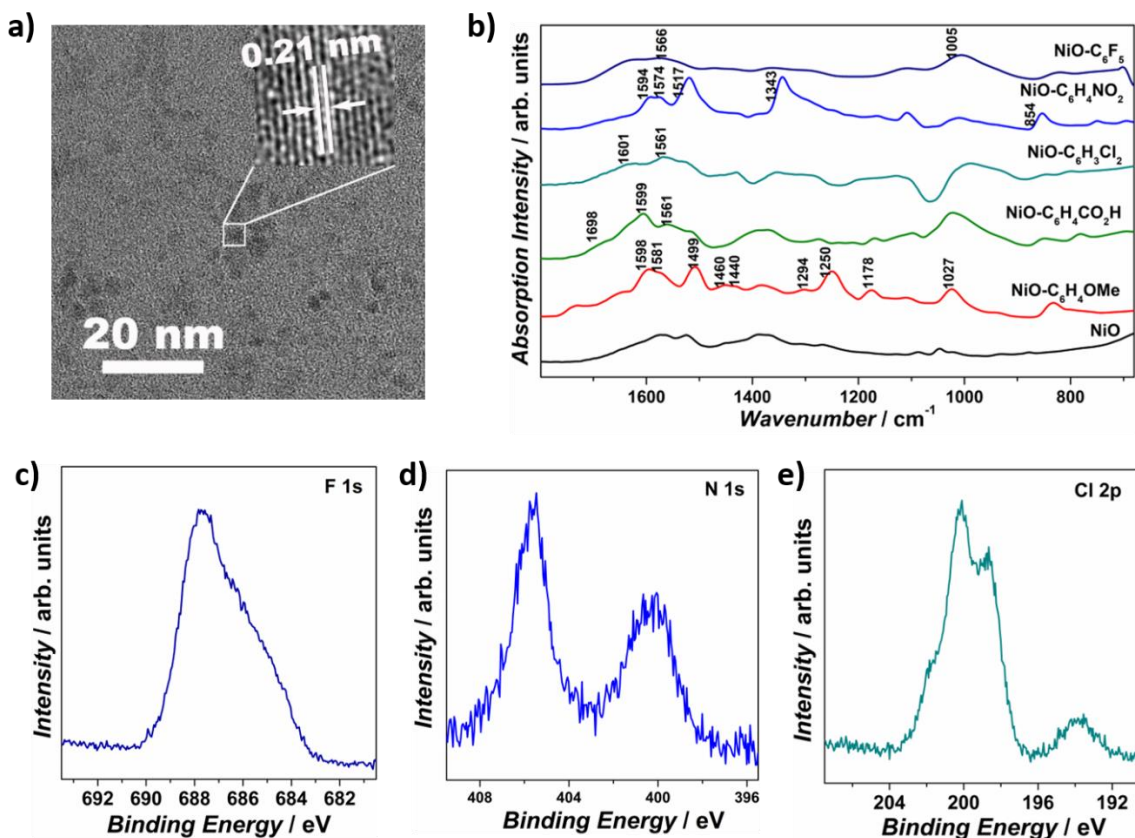


Figure 2 a) The TEM image of as-prepared ultrasmall NiO nanoparticles. b) DRIFTS spectra of bare NiO and all modified NiO samples. The high-resolution core XPS spectra of c) F 1s of NiO-C₆F₅, d) N 1s of NiO-C₆H₄NO₂ and e) Cl 2p of NiO-C₆H₃Cl₂.

Diffuse reflectance infrared Fourier transform spectroscopy (DRIFTS) was employed to study the molecular modification at NiO nanoparticle surface (Fig. 1b). All the modified NiO samples show additional characteristic peaks of the organic modification compared to bare NiO nanoparticles: the NiO-C₆F₅ spectrum shows C-F stretch at 1005 cm⁻¹;[10] the NiO-C₆H₄NO₂ spectrum shows NO₂ stretching and scissoring absorption modes at 1517, 1343 and 854 cm⁻¹;[8b, 10c] the NiO-C₆H₄CO₂H spectrum exhibits C=O stretching at 1698 cm⁻¹;[10c] and the NiO-C₆H₄OMe spectrum presents OMe stretches at 1460, 1440 cm⁻¹, Ar-O stretches at 1294, 1250 cm⁻¹, Ar-O-CH₃ stretch at 1027 cm⁻¹, O-CH₃ rocking mode at 1178 cm⁻¹. [8b, 10c] Aryl-groups related characteristic vibrations are also presented at 1550~1600 cm⁻¹ and 1450~1500 cm⁻¹ for all modified NiO samples, yet distinctly affected by the different electronic properties of substituents.[8b, 10c] The NiO-C₆H₄OMe sample presents a strong

absorption band at 1499 cm^{-1} , which is absent for other samples, consistent with the principle that this aryl-group IR band is only IR active when the aryl-group has an electron-donating substituent.^[8b, 10c] In $1550\sim 1600\text{ cm}^{-1}$ region, the NiO-C₆H₃Cl₂ and NiO-C₆F₅ samples show much lower peak intensity at 1601 cm^{-1} compared to the peak at 1564 cm^{-1} , in sharp contrast to NiO-C₆H₄NO₂ (comparable peak intensity at 1594 and 1574 cm^{-1}) and NiO-C₆H₄OMe, NiO-C₆H₄CO₂H (higher peak intensity at 1598 cm^{-1} compared to the peak at 1581 cm^{-1}).^[8b, 10c] The different electron-withdrawing strengths influence the symmetry of the phenyl stretch mode by altering the intrinsic dipole, inducing different IR absorption behavior.^[8b, 10c, 11]

UV-Vis absorption spectroscopy was conducted to approximate the loading of the organic modifications at the NiO nanoparticle surface (Fig. S12, S13, S14 and S15). By comparing the absorption intensity of the diazonium salt stock solutions before and after the grafting process, the functionalization amount of -C₆F₅, -C₆H₄NO₂, -C₆H₄CO₂H and -C₆H₄OMe were estimated to be 2.11, 2.55, 3.31 and 2.37 nm⁻², indicating their comparable coverage at the NiO surface.^[12] The molecular modification can be further confirmed by the XPS spectra of NiO-C₆F₅, NiO-C₆H₄NO₂ and NiO-C₆H₃Cl₂, which present distinct F, N and Cl signals respectively (Fig. 1c, 1d and 1e). Together with EDS and DRIFTS, these results demonstrate the successful molecular modification of the NiO by aryl-groups with comparable coverage.

Then, to investigate the electronic modulation by molecular modification, XPS was performed on all the modified samples. As shown in Fig. 3, the bare NiO sample shows Ni peaks at 856.1, 853.9 eV, and O peaks at 529.1, 531.2 eV, which can be attributed to the Ni²⁺-O and Ni²⁺-OH species,^[13] indicating the generation of Ni(OH)₂ at NiO surface when exposed to air.^[6a] Interestingly, the nickel oxide related Ni and O peaks were markedly shifted upon functionalization of the NiO particles. The NiO-C₆H₄OMe sample shows Ni peaks at 850.6 and 853.8 eV, O peak at 531.1 eV, which are 0.1 eV lower in energy compared with bare NiO, indicating the higher electron density on the surface Ni species.^[3a, 14] In contrast, the NiO-C₆H₄CO₂H, NiO-C₆H₃Cl₂, NiO-C₆H₄NO₂ samples show Ni peaks at 856.4 eV, O peaks at 531.6 eV, which show 0.3 eV and 0.4 eV shifts towards higher energy compared with the bare NiO, illustrating their decreased electron density around surface Ni species.^{[3a,}

^{14]} The strongest electron-withdrawing pentafluorophenyl-modified NiO sample shows a Ni peak at 856.7 eV, O peak at 531.7 eV, which are 0.6 eV and 0.5 eV positively shifted compared with bare NiO, presenting the highest value among all modified NiO samples. To sum up, the Ni and O binding energy increase with an order of $\text{NiO-C}_6\text{H}_4\text{OMe} < \text{NiO} < \text{NiO-C}_6\text{H}_4\text{CO}_2\text{H} \approx \text{NiO-C}_6\text{H}_3\text{Cl}_2 \approx \text{NiO-C}_6\text{H}_4\text{NO}_2 < \text{NiO-C}_6\text{F}_5$, demonstrating the successive electronic structure modulation by the varied electron-withdrawing abilities of $-\text{C}_6\text{H}_4\text{OMe} < -\text{C}_6\text{H}_4\text{CO}_2\text{H} \approx -\text{C}_6\text{H}_3\text{Cl}_2 \approx -\text{C}_6\text{H}_4\text{NO}_2 < -\text{C}_6\text{F}_5$.^[3a, 14a] All the molecular modified NiO samples show an additional peak in the O spectra in the range of 532.8 ~ 533.2 eV, which can be assigned to the O-C bond, indicating the formation of O-C bond linkage between NiO and the organic molecules.^[15]

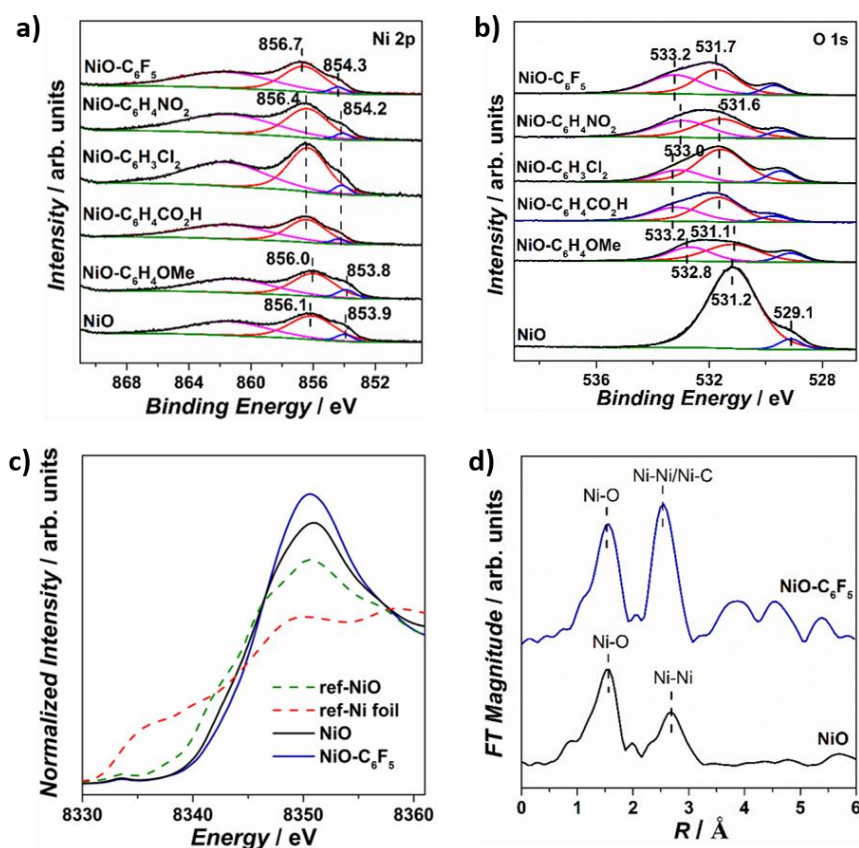


Figure 3 The high-resolution core XPS spectra of a) Ni2p and b) O1s of bare NiO and all modified NiO samples. c) Normalized Ni K-edge XANES spectra of NiO, NiO-C₆F₅, reference Ni foil and reference NiO samples. d) Fourier transformations of k^3 -weighted EXAFS spectra of bare NiO and NiO-C₆F₅ samples.

X-ray absorption of near-edge structure (XANES) and extended X-ray absorption fine structure (EXAFS) spectroscopy were performed on the strongest electron-withdrawing modified NiO-C₆F₅ samples to investigate its local structure. In XANES region, a characteristic pre-edge peak is presented at 8333 eV, which corresponds to the 1s to 3d transition of Ni in a disordered octahedral geometry (Fig. 3c). The absorption edge energy value (E_0) is comparable to that of reference NiO, indicating the Ni²⁺ oxidation state in the samples. The Fourier transformed k^3 -weighted EXAFS spectra presents two main peak maximums in the range of 1~3 Å (Fig. 3d). The first peak maximum can be attributed to the Ni-O backscattering path, which exhibits comparable radial distance (R) and coordination number (CN) for bare NiO and NiO-C₆F₅, in agreement with the disordered octahedral geometry of NiO₆ (Table S1).^[16] For the second peak maximum, two backscattering paths is required for the perfect peak fitting of NiO-C₆F₅, which can be attributed to the Ni---Ni and Ni---C backscattering. The R of Ni---Ni backscattering was fitted to be 2.97 Å for NiO-C₆F₅, lower than 3.10 Å of NiO, illustrating the structural disorder induced by the molecular modification. The CN of Ni---Ni backscattering path is fitted to be 7.96, much lower than the value of 12 in standard bulk NiO, indicating the exposure of coordinatively unsaturated sites at the nanoparticle surface.^[17] The CN and R of Ni---C backscattering was fitted to be 0.48 and 2.72 Å, which can be attributed to the Ni-O-C linkage between NiO and grafting molecules, confirming the molecular modification. Overall, these XPS and XAS results illustrate the systematical local electronic structure modulation of NiO nanoparticles by the simple molecular modification. The controlled electronic modulation is expected to directly tailor the Ni active species behavior and water oxidation activity.

Next, the electrocatalytic OER activity of bare NiO and modified NiO samples were evaluated under alkaline conditions (1M KOH) with glassy carbon electrode (GCE) as the working electrode (Fig. 4a). The bare NiO nanoparticles show an overpotential of 315 mV for reaching 1 mA/cm² current density and achieve 6.85 mA/cm² current density under 450 mV overpotential, consistent with its moderate activity towards OER.^[3b, 18] All the modified NiO samples exhibit distinctly altered OER activity, which is systematically affected by the molecular modification. The NiO-C₆H₄OMe sample requires 340 mV overpotential for 1 mA/cm² current density and achieves 5.62 mA/cm² current density under

450 mV overpotential, which presents a repressed catalytic activity compared to the bare NiO. In sharp contrast, the NiO-C₆H₃Cl₂, NiO-C₆H₄NO₂ and NiO-C₆F₅ samples show lower overpotential requirements of 293, 287 and 257 mV for 1 mA/cm² current density, and higher catalytic current densities of 13.17, 18.98 and 23.17 mA/cm² under 450 mV overpotential, demonstrating their sequentially improved OER activity. The NiO-C₆H₄CO₂H exhibits 310 mV overpotential for 1 mA/cm² and 8.93 mA/cm² current density under 450 mV overpotential, which is approximate to the bare NiO nanoparticles and can be related to the electron-neutral property of -C₆H₄CO₂⁻ under alkaline conditions.

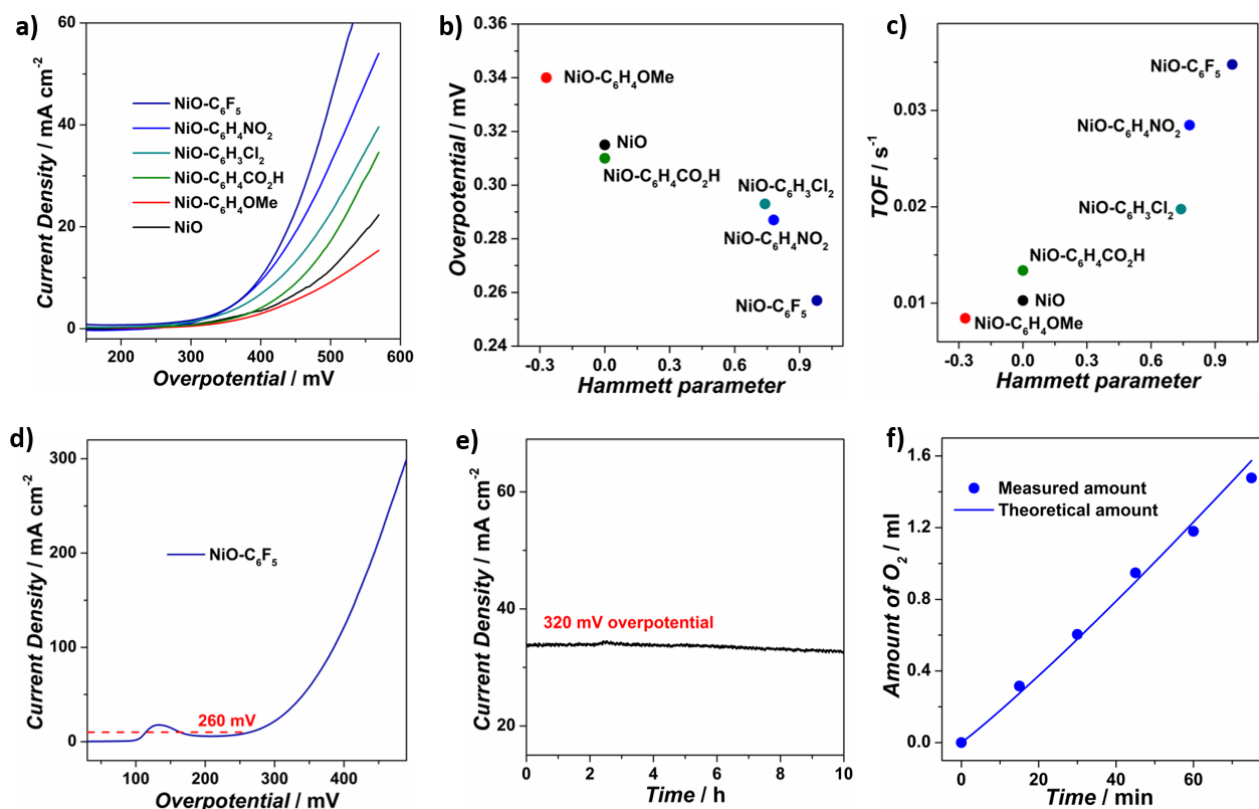


Figure 4 a) Polarization curves of bare NiO and modified NiO samples on glassy carbon electrode in 1M KOH. b) Overpotentials at 1 mA/cm² current density and c) Calculated TOFs at 450 overpotential of bare NiO and all modified NiO samples. d) Polarization curves of bare NiO and NiO-C₆F₅ on carbon fiber paper electrode in 1M KOH. e) Chronopotentiometric curve of NiO-C₆F₅ on carbon fiber

paper electrode at 320 mV overpotential. f) Quantification and comparison of the experimental and theoretical O₂ evolution amount by electrolysis of NiO-C₆F₅ for OER under 250 mV overpotential.

Turnover frequencies (TOF) were calculated by assuming that all the Ni ions are active sites (Fig. 4c and Table 1). The TOF values of NiO-C₆H₄CO₂H, NiO-C₆H₃Cl₂, NiO-C₆H₄NO₂ and NiO-C₆F₅ are calculated to be 0.013, 0.020, 0.028 and 0.035 s⁻¹, which are sequentially increased compared with 0.010 s⁻¹ for bare NiO and indicate their monotonically improved intrinsic activity. Conversely, NiO-C₆H₄OMe shows a decreased TOF value of 0.008 s⁻¹, showing a suppressed intrinsic activity compared to bare NiO. Tafel slopes were calculated by plotting overpotential against log (*J*) to obtain insight on the electrocatalytic OER kinetics (Fig. S17). The NiO-C₆H₄CO₂H, NiO-C₆H₃Cl₂, NiO-C₆H₄NO₂ and NiO-C₆F₅ samples show Tafel slopes of 126, 129, 89 and 87 mV/dec, which are beneficially decreased compared with 133 mV/dec of bare NiO, illustrating the accelerated OER kinetics. In contrast, the NiO-C₆H₄OMe sample shows a Tafel slope of 156 mV/dec, much higher than the native NiO nanoparticles and signifies the retardation of OER kinetics with electron-donating group. Altogether, the overpotential, current density, TOF and Tafel slope performances follow a similar OER activity trend with NiO-C₆H₄OMe < bare NiO ≤ NiO-C₆H₃CO₂H < NiO-C₆H₃Cl₂ < NiO-C₆H₄NO₂ < NiO-C₆F₅. By plotting the OER performances versus the Hammett sigma constants, a reasonable correlation can be presented between catalytic activity and the electronic properties of the modifying molecules: increasing electron-withdrawing strength readily decreases the electron density around surface Ni sites, accelerating catalytic kinetics and improving OER performance (Fig. 4b, 4c and S18).

Table 1 The summary of Hammett sigma constants and calculated TOF values under 450 mV overpotential of bare NiO and all molecule modified NiO samples on GCE.

Sample	NiO-C ₆ H ₄ OMe	NiO	NiO-C ₆ H ₄ CO ₂ H ^[a]	NiO-C ₆ H ₃ Cl ₂	NiO-C ₆ H ₄ NO ₂	NiO-C ₆ F ₅
Hammett Parameter	-0.27	0	0	0.74	0.78	0.98
TOF (s ⁻¹)	0.008	0.010	0.013	0.020	0.028	0.035

^[a] The -C₆H₄CO₂H group is deprotonated under alkaline conditions (-C₆H₄CO₂⁻), behaving as electron-neutral property.

The OER performance of the best catalyst, NiO-C₆F₅, was further evaluated on carbon fiber paper (CFP) as a 3D electrode substrate. The CFP/NiO-C₆F₅ electrode shows an overpotential of 260 mV for 10 mA/cm² current density (Fig. 4d). High current densities of 50 and 100 mA/cm² can be achieved for CFP/NiO-C₆F₅ by increasing the overpotential to 350 and 380 mV, confirming its prominent activity. In chronoamperometry measurements under 320 mV overpotential (Fig. 4e), no obvious deterioration in current density was observed during 10 h electrolysis, which indicates the excellent stability of the catalyst. This high stability is further confirmed by the TEM image of the NiO-C₆F₅ catalyst after long-term electrolysis, which indicated that nanoparticle size remained between 1-4 nm, displaying no apparent aggregation (Fig. S19). Typical F, Ni and O signals can be observed on the EDS spectrum, verifying the durability of the modified NiO-C₆F₅ catalyst. By comparison of experimental and theoretical O₂ evolution during electrolysis under 250 mV overpotential, the OER Faradaic efficiency was estimated to be 93.6% for the CFP/NiO-C₆F₅ electrode, indicating that the vast majority of consumed charges was contributed to catalytic water oxidation (Fig. 4f).

The above OER performance results illustrate that, through our simple covalent functionalization approach, the water oxidation activity is rationally tailored by the directed electronic modulation and an efficient NiO-C₆F₅ water oxidation catalyst is achieved with the adjusted molecular modification. Then, we perform a series of experiments to gain insightful understanding on the influence of -C₆F₅ modification on the activity.

Electrochemical surface area (ECSA) is one of the key factors that may be impacted by the surface molecular modification. The ECSA of bare NiO and NiO-C₆F₅ were estimated from their double-layer capacitance (*C_{dl}*) (Fig. S20 and S21). The linear slopes of NiO-C₆F₅ were calculated to be 0.16 mF/cm², close to 0.19 mF/cm² for bare NiO. This negligible difference in ECSA indicates that the molecular modification does not impact the active surface area of the catalyst.

The wettability of bare NiO and molecular modified NiO samples are evaluated by water contact angle measurement (Fig. S22). The NiO-C₆F₅ sample presents contact angle of 103.9°, which is higher than 77.7° of bare NiO. The decreased hydrophilicity of NiO-C₆F₅ can be attributed to the hydrophobicity

of grafted molecules. No clear correlation was observed between the hydrophily and OER performance, which indicate that the change of wettability cannot account for the significantly influenced activity.

Charge transfer also plays an essential role in water oxidation reaction at catalyst surface. To investigate the influence of molecular modification on charge transfer kinetics, electrochemical impedance spectroscopy (EIS) was conducted on NiO and NiO-C₆F₅ (Fig. 5a). The NiO-C₆F₅ sample shows a charge transfer resistance (R_{ct}) of 56.3 Ω , which is much lower compared with 152.4 Ω of bare NiO. The diminished resistance demonstrates that the -C₆F₅ molecular modification greatly facilitates the charge transfer kinetics.

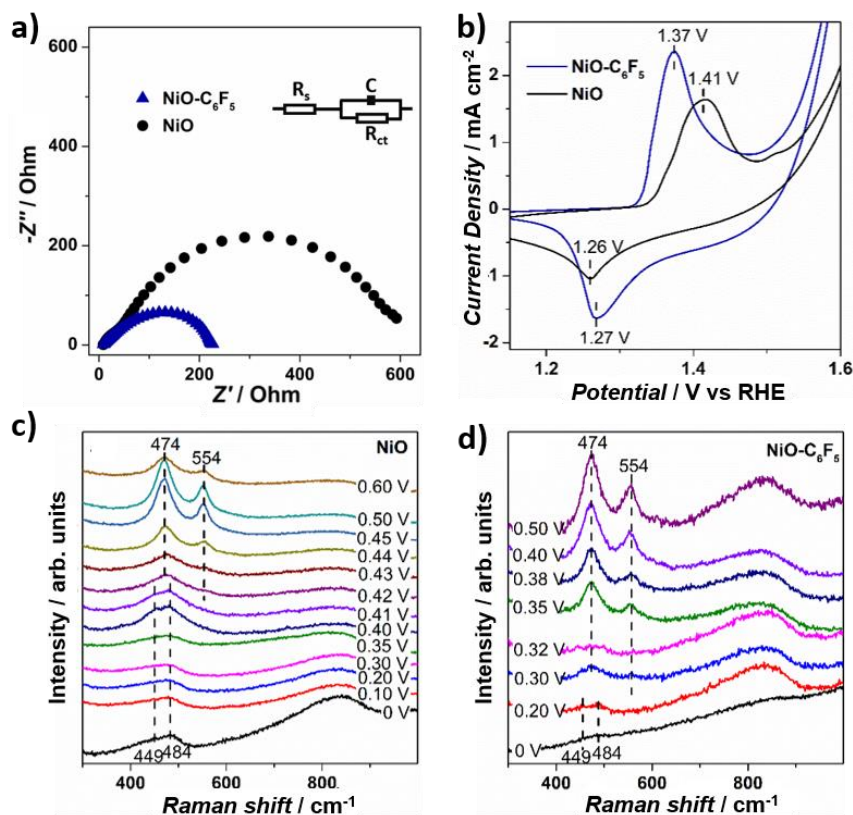


Figure 5 a) Nyquist diagram of NiO-C₆F₅ and NiO nanoparticles with a bias set at 350 mV overpotential. b) Cyclic voltammetry of bare NiO nanoparticles and the NiO-C₆F₅ sample at a scan

rate of 100 mV/s in 1 M KOH electrolyte. *Operando* Raman spectra of c) bare NiO and d) NiO-C₆F₅ samples under OER conditions.

A catalyst self-reconstruction of Ni²⁺ → NiOOH is reported to be commonly occurred at Ni-based water oxidation catalyst, generating γ -NiOOH as the surface active phase.^[5a, 19] To study the influence of molecular modification on the surface self-reconstruction, cyclic voltammetry (CV) was performed on bare NiO and NiO-C₆F₅ samples (Fig. 5b). The bare NiO sample shows a pair of redox peaks with an anodic peak (E_{a,p}) at 1.41 V, cathodic peak (E_{c,p}) at 1.26 V and mid-peak potential (E_{mid}=(E_{a,p}+ E_{c,p})/2) of 1.34 V, which can be attributed to the transformation of surface Ni²⁺ moieties to NiOOH active species.^[5a, 19] Notably, for NiO-C₆F₅, the anodic peak shows peak potential at 1.37 V, which is 40 mV lower compared with bare NiO, and the E_{mid} of the Ni redox peaks was calculated to be 1.32 V, 20 mV lower compared with bare NiO. The decrease peak potential indicate the promoted Ni²⁺ → NiOOH transformation in the NiO-C₆F₅ sample.^[3a, 5a, 18] Besides, along with the shift of the redox peak potential, the peak difference (ΔE_p) between the anodic and cathodic peaks was estimated to be 100 mV for NiO-C₆F₅, much lower compared with 150 mV of bare NiO, illustrating the accelerated transformation kinetics of Ni²⁺ → NiOOH on NiO-C₆F₅.^[20]

Then, *operando* Raman spectroscopy was further performed to investigate the relationship between molecular modification, active species behavior, and catalytic activity (Fig. 5c and 5d). Under 0 V potential (vs Ag/AgCl), both NiO and NiO-C₆F₅ samples show two vibration bands at 449 and 484 cm⁻¹, which can be attributed to the A_{1g} stretching modes of Ni-OH and Ni-O respectively.^[21] Upon increasing the applied potential, both samples present γ -NiOOH related bands at 474 and 554 cm⁻¹, yet the potential requirement is greatly altered.^[21a, 21d, 21e] For NiO-C₆F₅, the vibration bands at 474 and 554 cm⁻¹ started to appear at a potential of 0.30 V, which is 120 mV lower compared with 0.42 V of bare NiO. The maximum-steady state of these two bands was achieved at 0.40 V for NiO-C₆F₅, which is 40 mV less compared with 0.44 V of bare NiO. These decreased potential requirements clearly demonstrate the lower formation energy barrier of γ -NiOOH, illustrating the

facilitated generation of this active species at the of the NiO-C₆F₅ catalyst surface. Combined with the EIS and CV, we can conclude that the -C₆F₅ group modification effectively accelerates the charge transfer kinetics, promotes the catalyst reconstruction, and enhances the OER activity.^[5a, 19]

Although the catalytic mechanism of Ni-based OER catalysts remains a long-term scientific discussion, the formation of NiOOH species is accepted to play a pivotal role as the key intermediate in water oxidation. The nucleophilic addition of water molecules on the catalysts would be the first key step in the catalytic cycle. The electron-withdrawing modification can promote the local electron-delocalization at NiO surface, decreasing the electron density around the active Ni species and modulating the catalyst local structure. On one hand, the more electrophilic Ni site can favor the nucleophilic addition of water as well as the deprotonation in the Ni²⁺ → NiOOH reconstruction, achieving improved OER activity. On the other hand, with specific proton affinity, the -C₆F₅ group is proposed to promote proton shuttling at the catalyst surface, which can accelerate the deprotonation process, stimulate the generation of key intermediate, and improve the catalytic performance.^[22] Benefiting from the synergistic promotion effect, the NiO-C₆F₅ catalyst exhibits outstanding performance towards water oxidation. Further OER activity improvements and deeper mechanistic understanding can be achieved by directed molecular functionalization with optimized electronic properties.

Conclusion

In summary, we achieve directed electronic modulation of NiO through surface molecular modification, and thereby directly tailor the OER activity. By adjusting the electronic properties of the modifying molecules, the electronic environment around active sites is rationally modulated and the OER activity is systematically regulated: where the electron-withdrawing modification decreases the electron density at the surface Ni species and improves the OER activity, and vice versa. The strong electron-withdrawing -C₆F₅ molecular modification can effectively facilitate the charge transfer kinetics, promoting the reconstruction of Ni²⁺ moieties to the active γ -NiOOH phase, and thus greatly enhancing the OER performance. This work opens a new avenue for heterogeneous OER

catalyst design at the molecular level, demonstrating the significant impact of local electronic structure on the OER active species generation and catalytic activity.

Experimental Section:

Materials

Nickel(II) acetylacetonate ($\text{Ni}(\text{C}_5\text{H}_7\text{O}_2)_2$), anhydrous tert-butanol ($(\text{CH}_3)_3\text{COH}$), potassium hydroxide (KOH), 4-nitrobenzenediazonium tetrafluoroborate ($\text{C}_6\text{H}_4\text{N}_3\text{O}_2\text{BF}_4$), 3,5-dichlorophenyldiazonium tetrafluoroborate ($\text{C}_6\text{H}_3\text{Cl}_2\text{N}_2\text{BF}_4$), 4-methoxybenzenediazonium tetrafluoroborate ($\text{CH}_3\text{OC}_6\text{H}_4\text{N}_2\text{BF}_4$), 2,3,4,5,6-pentafluoroaniline ($\text{C}_6\text{F}_5\text{NH}_2$), nitrosyl tetrafluoroborate (NOBF_4), anhydrous acetone (CH_3COCH_3), anhydrous dichloromethane (CH_2Cl_2), and acetonitrile- d_3 (CD_3CN) were purchased from Sigma-Aldrich. 4-carboxylbenzenediazonium tetrafluoroborate ($\text{CO}_2\text{HC}_6\text{H}_4\text{N}_2\text{BF}_4$) was purchased from Chemtronica AB (Sweden). The water used for electrolyte solutions was deionized using a Millipore Milli-Q UF Plus system (15–18 $\text{M}\Omega\text{-cm}$ resistivity).

Synthesis of pentafluorophenyldiazonium tetrafluoroborate ($\text{C}_6\text{F}_5\text{N}_2\text{BF}_4$)

The pentafluorophenyldiazonium tetrafluoroborate was synthesized according to an available literature procedure.^[23] 5 mmol pentafluoroaniline was firstly dissolved in 1 ml acetonitrile, and then added dropwise over the course of 30 mins to a mixture of pulverized nitrosyl tetrafluoroborate (5 mmol, 915 mg) in dry acetonitrile (1 mL) at $-30\text{ }^\circ\text{C}$ in 30 min. After stirring at $-30\text{ }^\circ\text{C}$ for 1 h, 7.5 ml dry dichloromethane was added to the mixture. The desired pentafluorophenyldiazonium tetrafluoroborate could be obtained by filtration and drying in vacuum. ^{19}F NMR-spectroscopy confirms formation of the desired product: ^{19}F NMR (377 MHz, CD_3CN) δ -119.54 (tt, $J = 21.4$, 16.6 Hz), -123.43 (m), -151.31 (broad singlet, BF_4^-), -152.47 (m).

Synthesis of ultrasmall NiO nanoparticles

The ultrasmall NiO nanoparticles were synthesized following a reported solvothermal method.^[6a] 0.4 g $\text{Ni}(\text{acac})_2$ was firstly mixed with 35 ml tert-butanol under vigorous stirring at $50\text{ }^\circ\text{C}$ to form a suspension. The suspension was transferred into an autoclave reactor and hermetically sealed. The

reaction was performed by heating at 205 °C for 20 h. After the reaction, the ultrasmall nanoparticles were obtained by washing with ethanol for 3 times and drying at 80 °C.

Functionalization of NiO nanoparticles with organic molecule

The NiO nanoparticles were functionalized by suspending ~100 mg of NiO nanoparticles in Milli-Q water with 0.1 M NaOH under N₂ atmosphere, and then adding dropwise ~5 mL of a 10 mg/mL solution of the corresponding diazonium tetrafluoroborate salt: pentafluorophenyldiazonium tetrafluoroborate, 4-nitrobenzenediazonium tetrafluoroborate, 3,5-dichlorophenyldiazonium tetrafluoroborate, 4-carboxylbenzenediazonium tetrafluoroborate, or 4-methoxybenzenediazonium tetrafluoroborate. The mixed solutions were stirred overnight after which the products were collected by centrifugation and washing with water. The resulting functionalized NiO samples were obtained by drying under vacuum.

Physical characterization

Powder X-ray diffraction (XRD) was performed on Bruker D5000 X-ray diffraction diffractometer with Cu K α radiation ($\lambda = 1.5406 \text{ \AA}$). SEM images and EDS spectra were recorded with JEOL JSM 7401 equipped with an EDS system. TEM images and HRTEM images were taken on a JEOL JEM2100F transition electron microscope. Diffuse reflectance infrared Fourier transform spectroscopy (DRIFTS) spectra were measured on a Thermo Scientific Nicolet iS5 FT-IR spectrometer. UV-Vis spectra were carried on PerkinElmer Lambda 750 UV-Vis spectrophotometer. XPS spectra were acquired by a Thermo VG ESCALAB250 surface analysis system with monochromatized Al K α small-spot source and 500 μm concentric hemispherical energy analyzer. All the spectra energy was calibrated by setting the adventitious carbon peak to 284.6 eV.

Determination of the molecule loading amount

The degree of molecular modification was determined by the UV-Vis absorption method. A standard curve was obtained by plotting the UV-Vis absorption of stock solutions of the respective diazonium salts at different concentrations. The remaining concentration of diazonium salt of the solution after

NiO functionalization was determined based on their UV-Vis absorption intensity. The molecule loading amount was calculated by the difference between the initial molecular amount and the molecular concentration after NiO functionalization.

Electrode preparation

4 mg of the respective samples were dispersed in a mixed solution of 32 μL 5% Nafion (ethanol solution), 200 μL ethanol and 768 μL H_2O and sonicated for over 1 h to make a finely dispersed suspension. For glassy carbon electrodes (GCE), 10 μL of the obtained suspension was drop-casted on pre-polished GCE and the resulting electrodes were dried at 50 $^\circ\text{C}$ for 30 mins. For carbon fiber paper electrode (CFP), 100 μL of the catalyst suspension was drop-casted on pre-cleaned GFP electrode and the resulting electrodes were dried at 50 $^\circ\text{C}$ for 30 mins.

Electrochemical characterization

All electrochemical experiments were carried on a CH Instrument 660E potentiostat. The electrochemical cell was built by a three-electrode system with the as-prepared samples electrode as the working electrode, a standard Ag/AgCl electrode as the reference electrode and a platinum foil (4 cm^2) as the counter electrode. All the applied potentials were converted to reversible hydrogen electrode (RHE) using the equation $E(\text{vs. RHE}) = E(\text{vs. Ag/AgCl}) + 0.059\text{pH} + 0.197 \text{ V}$. The overpotential was calculated with equation $\eta = E(\text{vs. RHE}) - 1.23 \text{ V}$. For evaluation of the OER activity, linear sweep voltammetry (LSV) was performed from low initial potential to high final potential with a scan rate of 5 mV/s. 95% iR compensation was applied with the current interrupt method by the software supplied with the potentiostat. The Tafel slopes were calculated by plotting the overpotential η against $\log(j)$ from the LSV curves. Chronoamperometry measurement was performed to assess the durability of the catalyst. Cyclic voltammetry (CV) was operated under scan rate of 100mV/s to investigate the catalyst redox behavior. The catalytic turnover frequency (TOF) values are determined by the equation:

$$\text{TOF} = jA / (4Fm)$$

where j is the catalytic current density, A is the surface area of the electrode, F is the Faraday constant and m is the number of moles of the active sites. In this work, we assume that all the Ni ions are active sites for water oxidation. By catalyst loading amount calculation, the m is calculated to be 5.36×10^{-7} mole. The Faradaic efficiency was measured in a N₂-purged sealed cell. The quantity of O₂ gas evolution was determined every 15 mins by gas chromatography (Shimadzu GC-2014) every 15 mins. The Faradaic efficiency was calculated by the equation: Faradaic efficiency = $4F \times n_{O_2}/Q$, where F is Faraday constant, n_{O_2} is the measured O₂ amount and Q is the consuming charge amount. Electrochemical active surface areas (ECSA) were measured by the non-faradaic double-layer capacitance (C_{dl}) method. CV was performed at the potential window of 0-0.1 V vs. Ag/AgCl, with different scan rates of 30, 50, 70 and 90 mV/s. By plotting the $\Delta J = (J_a - J_c)$ at 0.05 V vs. Ag/AgCl against the scan rate, the linear slope which is twice of C_{dl} is used to represent ECSA. Electrochemical impedance spectroscopy (EIS) was carried out in the catalytic OER region with the frequency ranged from 0.1-10⁵ Hz under an applied potential of 1.58V.

XAS Data Analysis

The XAS spectra were measured at P-64 beamline, PETRA III, DESY, Hamburg. The samples and reference Ni foil were measured simultaneously in transmission mode. The data processing (pre-edge, post-edge background removal and normalization) and structural modelling (Fourier transformation and data fitting) were performed using EXAFS PAK.^[24] The k^3 -weighted EXAFS oscillations were analyzed by nonlinear least-squares fit of the data to the EXAFS equation. The various model parameters: average coordination number (CN), mean interatomic distances (R), Debye-Waller factor coefficients (σ^2), and threshold energy (E_0) were refined. The theoretical phases and amplitudes used in the refinements were calculated using the FEFF7.

In order to directly compare all of the NiO modified samples, a two shell model based on bulk NiO rock salt structure was used to fit the EXAFS data. The Fourier transform fitting of the EXAFS spectra was performed until ~ 3 Å which contains the main single scattering contributions. Hence, a single Ni-O scattering path was used to describe the 6 nearest neighboring oxygen atoms ($R_{eff} = 2.08$ Å) in the

first coordination shell. For fitting the second shell, a single Ni---Ni scattering path ($R_{\text{eff}} = 2.954 \text{ \AA}$) was used for both the samples. In addition, a third Ni---C scattering path ($R_{\text{eff}} = 2.72 \text{ \AA}$) was necessary to obtain a better fit in NiO-C₆F₅ (best fit in [Figure S16](#)). The S_0^2 was refined separately for each sample, while the number of single scattering paths for Ni-O, Ni---Ni and Ni---C as well as their lengths, and Debye-Waller factors were allowed to refine together. In the present study, the single scattering contributions up to $\sim 3 \text{ \AA}$ have been used for structural modelling and have been found sufficient to describe the local structure as reported in literature.^[25]

Operando Raman Spectra

Operando Raman spectra of bare NiO and NiO-C₆F₅ samples were collected by a confocal Raman microscope (RM 1000, Renishaw) under OER in an ambient air condition. The reference electrode and counter electrode were Ag/AgCl (3 M KCl) and Pt wire, respectively. The excitation source was emitted by a frequency doubled Nd: YAG laser with the wavelength of 532 nm. The power of laser through the Olympus 10x objective was about 12.5 mW measured by PM160T power meter. A grating of 1800 lines/mm was used for operando Raman tests. All operando Raman measurements were performed by a custom-made spectro-electrochemical cell, measuring the surface of the electrode from the side to avoid the bubble scattering. Each operando Raman spectra was recorded with an acquisition time of 10 s with 5-10 sweeps under current-time (i-t) measurement at a constant potential using a confocal Raman microscope coupled with a 90-degree angled Olympus 10x objective. The electrochemical cell was made of quartz and stood in front of the objective. All spectra were calibrated against the value of 520.7 cm^{-1} of a silicon wafer. The resolution of each spectra is 1 cm^{-1} .

Conflicts of interest

The authors declare no competing interest.

Acknowledgment

This work was financially supported by the Swedish Research Council (2017-00935), the Swedish Energy Agency, the Knut and Alice Wallenberg Foundation (KAW 2016.0072), the National Natural

Science Foundation of China (21120102036). The X-ray absorption experiments were performed at the Deutsches Elektronen-Synchrotron (DESY), PETRA III, P64. We sincerely thank Beamline scientists Dr. Wolfgang A. Caliebe and Dr. Akhil Tayal at P64, PETRA III, DESY, and Dr. Ning Yuan at Stockholm University for assistance with the XAS measurements. L. Fan, T. Liu and Q. Meng thank the China Scholarship Council (CSC) for Ph.D. student scholarship.

Reference

- [1] a) J. Song, C. Wei, Z.-F. Huang, C. Liu, L. Zeng, X. Wang, Z. J. Xu, *Chem. Soc. Rev.* **2020**, *49*, 2196-2214; b) B. Zhang, L. Sun, *Chem. Soc. Rev.* **2019**, *48*, 2216-2264.
- [2] a) N. T. Suen, S. F. Hung, Q. Quan, N. Zhang, Y. J. Xu, H. M. Chen, *Chem. Soc. Rev.* **2017**, *46*, 337-365; b) J. Gong, C. Li, M. R. Wasielewski, *Chem. Soc. Rev.* **2019**, *48*, 1862-1864.
- [3] a) L. Fan, P. Zhang, B. Zhang, Q. Daniel, B. J. J. Timmer, F. Zhang, L. Sun, *ACS Energy Lett.* **2018**, *3*, 2865-2874; b) M. Gong, Y. Li, H. Wang, Y. Liang, J. Z. Wu, J. Zhou, J. Wang, T. Regier, F. Wei, H. Dai, *J. Am. Chem. Soc.* **2013**, *135*, 8452-8455; c) X. Xu, F. Song, X. Hu, *Nat. Commun.* **2016**, *7*, 12324; d) R. Liu, Y. Wang, D. Liu, Y. Zou, S. Wang, *Adv. Mater.* **2017**, *29*, 1701546; e) K. Fan, H. Chen, Y. Ji, H. Huang, P. M. Claesson, Q. Daniel, B. Philippe, H. Rensmo, F. Li, Y. Luo, L. Sun, *Nat. Commun.* **2016**, *7*, 11981.
- [4] a) S. Lee, K. Banjac, M. Lingenfelder, X. Hu, *Angew. Chem.* **2019**, *131*, 10401-10405; *Angew. Chem. Int. Ed.* **2019**, *58*, 10295-10299; b) M. Gorlin, P. Chernev, J. Ferreira de Araujo, T. Reier, S. Dresch, B. Paul, R. Krahnert, H. Dau, P. Strasser, *J. Am. Chem. Soc.* **2016**, *138*, 5603-5614; c) B. M. Hunter, N. B. Thompson, A. M. Müller, G. R. Rossman, M. G. Hill, J. R. Winkler, H. B. Gray, *Joule* **2018**, *2*, 747-763.
- [5] a) T. Wu, S. Sun, J. Song, S. Xi, Y. Du, B. Chen, W. A. Sasangka, H. Liao, C. L. Gan, G. G. Scherer, L. Zeng, H. Wang, H. Li, A. Grimaud, Z. J. Xu, *Nat. Catal.* **2019**, *2*, 763-772.; b) Y. Duan, S. Sun, Y. Sun, S. Xi, X. Chi, Q. Zhang, X. Ren, J. Wang, S. J. H. Ong, Y. Du, L. Gu, A. Grimaud, Z. J. Xu, *Adv. Mater.* **2019**, *31*, 1807898.
- [6] a) K. Fominykh, J. M. Feckl, J. Sicklinger, M. Döblinger, S. Böcklein, J. Ziegler, L. Peter, J. Rathousky, E.-W. Scheidt, T. Bein, D. Fattakhova-Rohlfing, *Adv. Funct. Mater.* **2014**, *24*, 3123-3129; b) K.

- Fominykh, P. Chernev, I. Zaharieva, J. Sicklinger, G. Stefanic, M. Döblinger, A. Müller, T. Pokharel, S. Böcklein, C. Scheu, T. Bein, D. Fattakhova-Rohlfing, *ACS Nano* **2015**, 9, 5180-5188.
- [7] a) K. Thamaphat, P. Limsuwan, B. Ngotawornchai, *Nat. Sci.* **2008**, 42, 357-361; b) R. Banerjee, R. Jayakrishnan, P. Ayyub, *J. Phys.: Condens. Matter.* **2000**, 12, 10647–10654.
- [8] a) V. Biju, *Chem. Soc. Rev.* **2014**, 43, 744-764; b) E. E. Benson, H. Zhang, S. A. Schuman, S. U. Nanayakkara, N. D. Bronstein, S. Ferrere, J. L. Blackburn, E. M. Miller, *J. Am. Chem. Soc.* **2018**, 140, 441-450; c) A. Chaussé, M. M. Chehimi, N. Karsi, J. Pinson, F. Podvorica, C. Vautrin-Ul, *Chem. Mater.* **2002**, 14, 392-400; d) K. Brymora, J. Fouineau, A. Eddarir, F. Chau, N. Yaacoub, J.-M. Grenèche, J. Pinson, S. Ammar, F. Calvayrac, *J. Nanopart. Res.* **2015**, 17, 438; e) R. Bangle, R. N. Sampaio, L. Troian-Gautier, G. J. Meyer, *ACS Appl. Mater. Inter.* **2018**, 10, 3121-3132; f) N. Griffete, F. Herbst, J. Pinson, S. Ammar, C. Mangeney, *J. Am. Chem. Soc.* **2011**, 133, 1646-1649; g) L. Xie, X. Li, B. Wang, J. Meng, H. Lei, W. Zhang, R. Cao, *Angew. Chem.* **2019**, 131, 19059-19063; *Angew. Chem. Int. Ed.* **2019**, 58, 18883-18887.
- [9] a) C. Hansch, A. Leo, R. W. Taft, *Chem. Rev.* **1991**, 91, 165-195; b) J. Mille, W. H. Yeung, *Amt. J. Chem.* **1967**, 2, 379-381; c) A. W. Sheppard, *J. Am. Chem. Soc.* **1970**, 92, 5419-5422.
- [10] a) S. R. Sellevåg, T. Kelly, H. Sidebottom, C. J. Nielsen, *Phys. Chem. Chem. Phys.* **2004**, 6, 1243-1252; b) Z. Liang, W. Chen, J. Liu, S. Wang, Z. Zhou, W. Li, G. Sun, Q. Xin, *J. Membr. Sci.* **2004**, 233, 39-44; c) D. Lin-Vien, N. B. Colthup, W. G. Fateley, J. G. Grasselli, *The Handbook of Infrared and Raman Characteristic Frequencies of Organic Molecules*. Elsevier, **1991**.
- [11] S. M. Jain, S. Tripathi, S. Tripathi, G. Spoto, T. Edvinsson, *RSC Adv.* **2016**, 6, 104782-104792.
- [12] a) L. Doub, J. M. Vandenbelt, *J. Am. Chem. Soc.* **1947**, 69, 2714-2723; b) L. Doub, J. M. Vandenbelt, *J. Am. Chem. Soc.* **1949**, 71, 2414-2420.
- [13] Q. Ke, C. Guan, M. Zheng, Y. Hu, K.-h. Ho, J. Wang, *J. Mater. Chem. A* **2015**, 3, 9538-9542.
- [14] a) L. Fan, J. Long, Q. Gu, H. Huang, H. Lin, X. Wang, *J. Catal.* **2014**, 320, 147-159; b) M. Scheffler, C. Stampfl, E. K. Horn, *Handbook of Surface Science* **2000**, 2, 749-862; c) G. Greczynski, L. Hultman, *Prog. Mater. Sci.* **2020**, 107, 100591; d) K. Siegbahn, *Electron Spectroscopy for Chemical Analysis*,

- In: S.J. Smith, G.K. Walters (eds) *Atomic Physics 3*, Springer, Boston, MA. **1973**; e) I. Lindgren, *J Electron Spectros. Relat. Phenomena* **2004**, 137-140, 59-71.
- [15] a) D. R. Bae, W. S. Han, J. M. Lim, S. Kang, J. Y. Lee, D. Kang, J. H. Jung, *Langmuir* **2010**, 26, 2181-2185; b) F. Soderlind, H. Pedersen, R. M. Petoral, Jr., P. O. Kall, K. Uvdal, *J. Colloid Interface Sci.* **2005**, 288, 140-148.
- [16] A .N. Mansour, C. A. Melendres, *J. Phy. Chem. A* **1998**, 102, 65-81.
- [17] a) M. A. Peck, M. A. Langell, *Chem. Mater.* **2012**, 24, 4483-4490; b) Y. Zhu, H. Guo, Y. Wu, C. Cao, S. Tao, Z. Wu, *J. Mater. Chem. A* **2014**, 2, 7904-7911.
- [18] M. B. Stevens, C. D. M. Trang, L. J. Enman, J. Deng, S. W. Boettcher, *J. Am. Chem. Soc.* **2017**, 139, 11361-11364.
- [19] O. Diaz-Morales, D. Ferrus-Suspedra, M. T. M. Koper, *Chem. Sci.* **2016**, 7, 2639-2645.
- [20] a) Q. Yang, Y. Nie, X. Zhu, X. Liu, G. Li, *Electrochim. Acta* **2009**, 55, 276-280; b) N. Elgrishi, K. J. Rountree, B. D. McCarthy, E. S. Rountree, T. T. Eisenhart, J. L. Dempsey, *J. Chem. Edu.* **2017**, 95, 197-206.
- [21] a) M. W. Louie, A. T. Bell, *J. Am. Chem. Soc.* **2013**, 135, 12329-12337; b) B. J. Trzesniewski, O. Diaz-Morales, D. A. Vermaas, A. Longo, W. Bras, M. T. Koper, W. A. Smith, *J. Am. Chem. Soc.* **2015**, 137, 15112-15121; c) S. Lee, K. Banjac, M. Lingenfelder, X. Hu, *Angew. Chem.* **2019**, 131, 10401-10405; *Angew. Chem. Int. Ed.* **2019**, 58, 10295-10299; d) Z. Qiu, C.-W. Tai, G. A. Niklasson, T. Edvinsson, *Energ. Environ. Sci.* **2019**, 12, 572-581; e) K. Zhu, X. Zhu, W. Yang, *Angew. Chem.* **2019**, 131, 1264-1277; *Angew. Chem. Int. Ed.* **2019**, 58, 1252-1265.
- [22] a) A. Yamaguchi, R. Inuzuka, T. Takashima, T. Hayashi, K. Hashimoto, R. Nakamura, *Nat. Commun.* **2014**, 5, 4256; b) W. Li, F. Li, H. Yang, X. Wu, P. Zhang, Y. Shan, L. Sun, *Nat. Commun.* **2019**, 10, 5074.
- [23] S. K. Fehler, G. Pratsch, C. Östreicher, M. C. D. Fürst, M. Pischetsrieder, M. R. Heinrich, *Tetrahedron* **2016**, 72, 7888-7893.
- [24] G. N. George, I. J. Pickering, "EXAFSPAK—A Suite of Computer Programs for Analysis of X-ray Absorption spectra, SSRL." **1993**.

- [25] a) F. Zhuang, J. C. Tang, J. P. He, L. Wang, *Phys. Chem. Chem. Phys.* **2000**, 2, 3571-3575; b) A. K. Agegnehu, C.-J. Pan, J. Rick, J.-F. Lee, W.-N. Su, B.-J. Hwang, *J. Mater. Chem.* **2012**, 22, 13849-13854; c) A. Anspoks, A. Kalinko, R. Kalendarev, A. Kuzmin, *Phys. Rev. B* **2012**, 86, 174114.

